Available online at www.sciencedirect.com
ScienceDirect
Catalysis Today 120 (2007) 413–419
CATALYSIS TODAY
www.elsevier.com/locate/cattod

Graphite nanofibers prepared from catalytic graphitization of electrospun poly(vinylidene fluoride) nanofibers and their hydrogen storage capacity

Sung Eun Hong [a,b], Dong-Kyu Kim [a], Seong Mu Jo [a,*], Dong Young Kim [a], Byung Doo Chin [a], Do Weon Lee [b]

[a] *Opoelectronic Materials Research Center, Korea Institute of Science and Technology, 39-1, Hawolgok-dong, Seongbuk-gu, Seoul 136-791, Republic of Korea*
[b] *Department of Chemical Engineering, University of Seoul, Jeonnong-Dong, Dongdeamun-Gu, Seoul 130-743, Republic of Korea*

Available online 13 November 2006

Abstract

Electrospun poly(vinylidene fluoride) nanofibers were carbonized with iron(III) acetylacetonate to induce catalytic graphitization within the temperature range 800–1800 °C. Carbonization in the presence of the catalyst produced graphite nanofibers (GNFs). Their structural properties and morphology were investigated. GNFs with a high surface area of 377–473 m^2/g showed the typical Type II containing mesopore in nitrogen adsorption–desorption isotherms. The hydrogen storage capacity of these GNFs was evaluated by the gravimetric method using a magnetic suspension balance (MSB) at room temperature and about 80 bar. The hydrogen storage capacity was 0.11–0.18 wt.%. The effective pore size for hydrogen storage compared to the diameter of the hydrogen molecule is discussed.

Keywords: Electrospun poly(vinylidene fluoride) nanofiber; Catalytic graphitization; Graphitic nanofiber; Hydrogen storage; Adsorption

1. Introduction

Since Dillon et al. first reported the excellent hydrogen storage capacity of single-wall nanotubes (SWNTs) at room temperature and atmospheric pressure [1], several studies of hydrogen storage using SWNTs, multi-wall nanotubes (MWNTs), graphite nanofibers (GNFs), active carbon, active carbon fibers, etc., have been conducted. Zhu et al. reported a hydrogen adsorption of approximately 3 wt.% at 3–100 MPa and room temperature using a well-aligned SWNT bundle [2]. On the other hand, purified SWNT (285 m^2/g) and saran carbon (1600 m^2/g) with a high BET surface area were also reported to have a hydrogen adsorption of approximately 0.04 and 0.28 H/C, respectively, at 0.32 MPa and 80 K [3]. Nijkamp et al. [4] also reported large hydrogen adsorption by a microporous zeolite and active carbons at 77 K and atmospheric pressure. Chahine and Bose [5] reported very high hydrogen adsorption of 5.3 wt.% (0.64 H/C) at 77 K and 1 MPa for highly porous carbon (AX-21 carbon). Despite the large volume of data from studies conducted on SWNTs, MWNTs, GNFs, etc., as potent hydrogen storage materials, these data are scattered and are thus inconclusive. SWNTs in more accurate volumetric measurements showed low capacity within the range of 0.14–0.43 wt.% and results for MWNTs and graphite powder were less than 0.04 wt.% [6]. Typical carbon materials, such as active carbon, active carbon fibers, and graphite powder, were also investigated as potent materials for hydrogen storage [5,7]. Active carbon materials with very high surface areas have very low capacities at room temperature. The hydrogen storage capacity of saran carbon is higher than that of other active carbon materials [3]. The potential fields from opposite walls overlap so that the attractive force acting on hydrogen molecules is greater than that on an open flat surface. In microporous carbon materials the pores with a width not exceeding a few hydrogen molecules are thought to be more effective for hydrogen storage compared to the dynamic

* Corresponding author. Tel.: +82 2 958 5355; fax: +82 2 958 5309.
E-mail address: smjo@kist.re.kr (S.M. Jo).

0920-5861/$ – see front matter © 2006 Elsevier B.V. All rights reserved.
doi:10.1016/j.cattod.2006.09.013

diameter of hydrogen molecule (0.4059 nm) [8]. PVdF and sarane polymers can be used in obtaining mesoporous carbon [9]. The pore size of the resulting material may be smaller than that of saran carbon because of the small size of the fluorine atom.

The recent electrospinning process for polymer solutions is a powerful method for producing ultrafine polymer fibers within the range of a few to a few hundred nanometers in diameter, which cannot be easily obtained using traditional methods [10]. Nano-sized fibers may be more helpful in obtaining carbon materials with a well-defined pore structure compared to the carbonization of micro-sized polymer fibers. Thus, such electrospun polymeric nanofibers may be used as effective precursors of carbon nanofibers. In addition, a transition metal would promote degree of graphitization during carbonization of the polymeric precursor, which has been verified for Kapton films by various research groups [11,12]. Recently, we reported the effects of iron(III) acetylacetonate (IAA) on the carbonization behavior of electrospun polyimide and polyacrylonitrile (PAN) nanofibers resulting in GNFs [13,14]. In addition, the carbonization of electrospun PVdF nanofibers with an average fiber diameter of 200–300 nm produced microporous carbon nanofibers with much higher surface areas than the PAN-based GNFs. The hydrogen storage capacity, however, was much lower than that of PAN-based GNFs [15,16].

In this study, GNFs with a high surface area were prepared through the catalytic graphitization of electrospun PVdF-based nanofibers containing IAA. Their structural properties, morphology, and effective pore for hydrogen storage were discussed.

2. Experimental

A PVdF solution was obtained by dissolving 11 wt.% of PVdF (Kynar 761, Elf AtoChem) in 100 ml of acetone/*N*,*N*-dimethylacetamide (7:3, w/w) mixture containing 25 μl of 1,8-diazabicyclo[5.4.0]undec-7-ene for partial dehydrofluorination. The PVdF solution also contained 5.5 wt.% of IAA based on the weight of the polymer as a catalyst for graphitization. PVdF-based nanofibrous membranes were prepared using typical electrospinning of the above PVdF solution.

The resulting electrospun PVdF-based nanofibrous membranes were chemically dehydrofluorinated with a 4 M aqueous NaOH solution containing 0.25 mmole of tetrabutylammonium bromide at 70 °C for 1 h.

Carbonization was performed to induce micropore structures without a further activation process at a given temperature within the range 800–1800 °C under a nitrogen atmosphere. The samples were heated at a rate of 3 °C/min and were maintained for 1 h at the final temperature.

The surface morphology of resulting GNFs was observed by scanning electron microscopy (SEM). Wide-angle X-ray scattering (WAXS) patterns were obtained using an X-ray diffractometer with Cu Kα radiation within the range $2\theta = 10$–80°. Raman spectra were obtained using Micro-Raman equipment with argon. Nitrogen gas adsorption–desorption isotherms were measured using an automatic gas adsorption apparatus (Themo, Sorptomatic 1990). The BET surface areas were calculated from the adsorption isotherms. The pore size distribution was obtained by applying the Horvath Kawazoe pore sizes for microporous samples and the B.J.H. pore sizes for mesoporous samples.

The hydrogen storage capacity of GNFs was evaluated by the gravimetric method using a magnetic suspension balance (MSB, Rubotherm). The blank test chamber containing samples was evacuated to remove impurities and water, and was run at 150 °C and 10^{-6} Torr for 6 h. The weight of the sample basket and sample was then measured at 10^{-6} Torr and 25 ± 0.5 °C and at a He gas atmosphere of 10 bar, respectively.

The weight difference between the vacuum and the 10-bar He gas, which indicates buoyancy due to the He gas, was used to determine the volume of the carbon nanofiber samples, as follows:

$$V_s = \frac{\Delta W_1}{d_{He}}, \quad (1)$$

where V_s is the volume of the samples, ΔW_1 the weight difference of the samples between the vacuum and the 10-bar He gas atmosphere, and d_{He} is the density of He at a specific pressure and temperature. It was assumed that He gas was not adsorbed by the GNFs in this condition.

The weights of the samples were measured under different H_2 pressures (0–80 bar) at 25 °C (±0.5 °C). The weights of the absorbed hydrogen were determined after the correction of the buoyancy due to the hydrogen gas atmosphere, using the sample volume (V_s), as follows:

$$\text{The weight of the adsorbed} H_2 = \Delta W_2 + V_s d_{H_2}, \quad (2)$$

where ΔW_2 is the weight difference of the samples between the vacuum and the specific H_2 pressure, V_s the volume of the samples, and d_{H_2} is the density of H_2 at a specific pressure and temperature. The densities of He and H_2 gas for buoyancy correction were calculated from a real gas equation using the Thermodynamic and Transport Properties of Pure Fluid Program (NIST-supported). As shown in Table 1, the of buoyancy is about 1 wt.% of GNFs, calculated according to the Eq. (2).

3. Results and discussion

Microporous carbon nanofibers could be obtained through the carbonization of PVdF nanofibers without further activation.

Table 1
Effects of buoyancy on GNFs at given temperature and pressure of H_2, compared to weight of the GNFs samples

Carbonization temperature (°C)	Weight of samples (g)	Pressure of H_2 (bar)/ temperature (°C)	Buoyancy ($V_s d_{H_2}$)	
			A (wt.%)	*B* (wt.%)
GNF				
800	0.316210	80.4/24.6	1.05	1.00
1000	0.285305	80.0/24.7	1.07	1.02

A: buoyancy calculated using ideal gas state equation, compared to weights of GNF samples; B: buoyancy calculated using real gas state equation (NIST), compared to weights of GNF samples; V_s: volume of sample; d_{H_2}: density of hydrogen gas.

PVdF nanofibers containing IAA as a catalyst for graphitization should be infusible to maintain their fibrous shape during carbonization through the dehydrofluorination reaction. In this study, dehydrofluorination was carried out with 4 M aqueous NaOH solution containing 0.25 mmole of tetrabutylammonium bromide at 70 °C for 1 h. The weight reduction of the nanofibers by chemical dehydrofluorination was 27 wt.%, indicating the removal of about 0.86 mole of HF per $–CH_2CF_2–$ repeat unit of PVdF. The chemically dehydrofluorinated nanofibers, however, still had 1.14 mole of HF per PVdF repeat unit, which corresponds to 48.7 wt.% of dehydrofluorinated PVdF nanofiber. Fig. 1 shows TGA curve of the above dehydrofluorinated PVdF nanofiber at a heating rate of 10 °C/min and the weight losses of dehydrofluorinated PVdF nanofiber samples after carbonization in the furnace at heating rate of 3 °C/min, which were 59 wt.% (800 °C), 59 wt.% (1000 °C), 62 wt.% (1300 °C), 64 wt.% (1500 °C), and 68 wt.% (1800 °C). Dramatic weight losses in the TGA curve occurred twice, at approximately 400 and 750 °C. The weight loss at approximately 400 °C was mainly due to the removal of HF and F fractions, and that at approximately 750 °C to the evolution of hydrocarbons from the PVdF. In the case of carbonization in the furnace in the temperature range 800–1800 °C weight loss was only 9 wt.%. This assumed that volatile hydrocarbon fractions were used as a carbon source for catalytic graphitization and thus the weight loss during carbonization was minimized. The weight loss in TGA was much faster than that in the furnace. This may suggest that the loss of volatile hydrocarbon fractions was faster than the reaction rate of catalytic graphitization because of the fast heating rate.

The morphology of PVdF-based carbon nanofibers greatly depends on the extent of the dehydrofluorination [16]. A high degree of dehydrofluorination produces very smooth surfaces and dense, non-porous carbon nanofibers (CNFs) that show a disordered crystal structure. In the case of the PVdF nanofibers that were partially dehydrofluorinated, carbonization produced porous CNFs with a high surface area. They also showed disordered carbon, regardless of the carbonization temperature. The pore structure became dense with increasing carbonization temperature, indicating the formation of micropores at higher carbonization temperatures. However, this did not indicate high hydrogen storage capacity, because micropores with a width not exceeding 1 nm are thought to be much more effective for hydrogen storage when considered with the dynamic diameter of the hydrogen molecule of approximately 0.4059 nm [8].

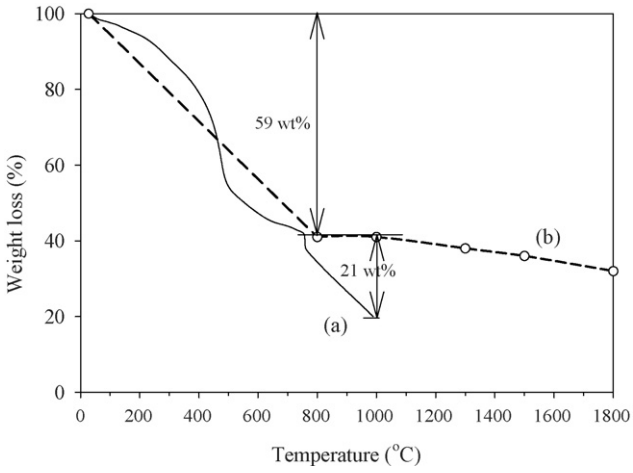

Fig. 1. Results for chemically dehydrofluorinated nanofibers: (a) thermogravimetric analysis (TGA) using a heating rate of 10 °C/min and (b) carbonization using a heating rate of 3 °C/min in the furnace.

Catalytic graphitization of volatile hydrocarbon fractions during the carbonization may be helpful in increasing the carbon yield and in forming effective ultramicropores for hydrogen storage. In this study, electrospun PVdF nanofibers were carbonized with IAA to induce catalytic graphitization within the range 800–1800 °C under a nitrogen atmosphere. Fig. 2 shows SEM images of PVdF-based GNFs. The surface and cross-section images of the GNFs show a notable grainy structure. The partial dehydrofluorination of PVdF nanofibers induced inhomogeneous structures consisting of a dehydrofluorinated amorphous region and an unreacted crystalline region. The crystalline region melted at a high temperature, while the dehydrofluorinated region maintained its fibrous shape during the carbonization. The onset temperature and the volume reduction during carbonization differed between the unreacted and reacted regions [9]. Thus, relatively large pores were produced between these regions. Therefore, carbonization of the partially dehydrofluorinated PVdF nanofibers induced porous GNFs with a high surface area due to their porous granular surface. The carbon granules in Fig. 2 may be with a well-defined graphite structure. Pyrolysis of hydrocarbon polymers having a linear chain structure with the same chemical bonding involving sp^2 hybrid orbitals, such as polyacetylene (PA), is known to produce hollow spheres with a graphitic structure [17].

Fig. 3a–d shows TEM images of PVdF-based GNFs. Clusters of Fe catalyst and the development of graphite structures centered on the Fe catalyst are clearly observed in Fig. 3a; the size of the Fe catalyst is from a few tens to a few hundreds of nanometers. Fig. 3 also shows the hollow structure with a well-defined graphite layered sphere, although the shapes are irregular. The net structure of these carbon nanofibers consists of a graphite-like structure, which forms a turbostratic-oriented graphite layer. Generally, this type of structure has been obtained from carbonization of rigid polymers such as Kapton imide [18]. However, the electrospun thermoplastic nanofibers also transformed to form a well-ordered graphite structure similar to natural graphite through catalytic graphitization during carbonization.

Fig. 4 shows XRD patterns for PVdF-based GNFs with carbonization temperature. Even at 800 °C, the GNFs show sharp peaks at approximately 26° and 44°, corresponding to the diffraction of the (0 0 2) plane and (1 0 0)/(1 0 1) of the graphite structure, respectively. The presence of the (1 1 2) peak at 83° is also indicative of a graphite structure. The intensities of these peaks increased and sharpened with the carbonization temperature. The catalytic graphitization of PVdF nanofibers containing IAA intensively proceeded from 800 °C. New peaks also appeared at 36° and 48°, corresponding to Fe_3O_4. It was assumed that IAA was converted into Fe_3O_4 *via*

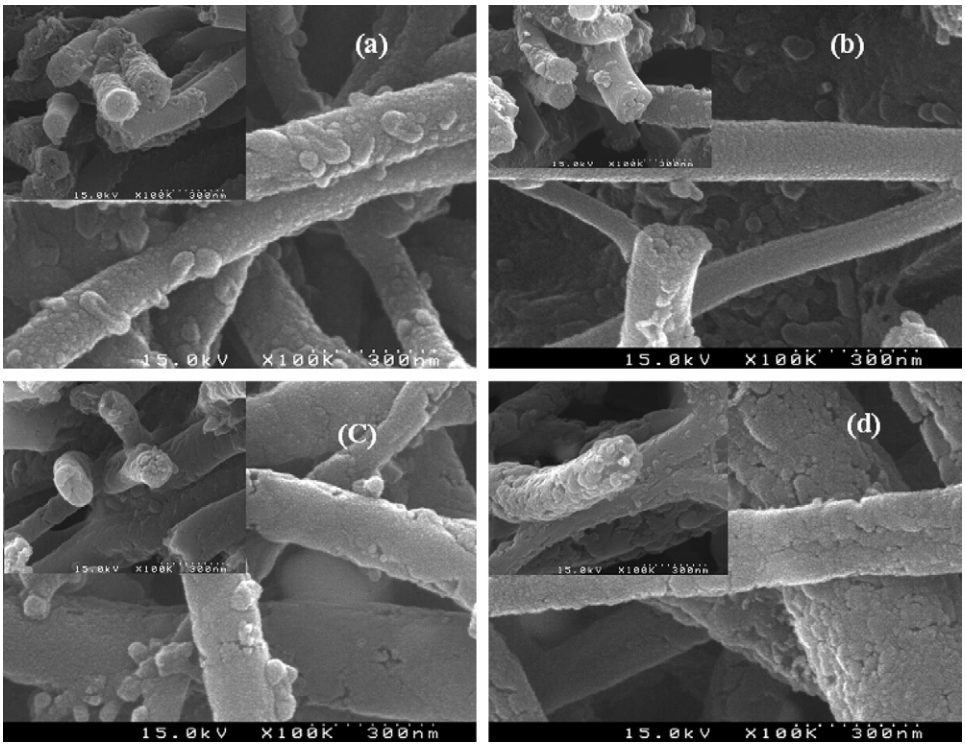

Fig. 2. SEM images of electrospun PVdF-based graphitic carbon nanofibers. Carbonization temperature: (a) 800 °C; (b) 1000 °C; (c) 1500 °C; (d) 1800 °C.

α-FeO (OH) during carbonization, and that the reduction of Fe_3O_4 resulted in production of the α-Fe catalyst that could induce the graphitization reaction. In the case of GNFs above 1300 °C, most of the Fe_3O_4 was transformed to α-Fe. As shown in Fig. 4, GNFs prepared at 1500 °C obviously showed α-Fe peaks at approximately 42–44° (1 1 0) and 65° (2 0 0). The $d_{0\,0\,2}$ values are in the range 0.333–0.343 nm, approaching the value for graphite. The values of $d_{0\,0\,2}$ indicate that the PVdF-based GNFs have a turbostratic structure because they were not entirely composed of a graphite structure, as shown in Fig. 3.

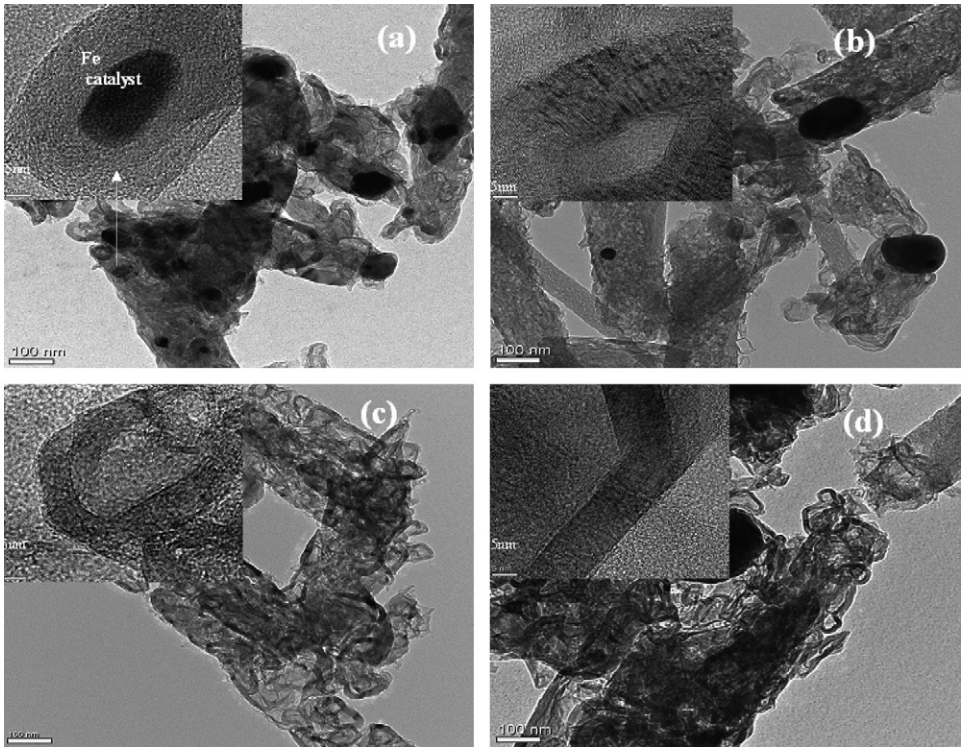

Fig. 3. TEM images of electrospun PVdF-based graphitic carbon nanofibers. Carbonization temperature: (a) 800 °C; (b) 1000 °C; (c) 1500 °C; (d) 1800 °C.

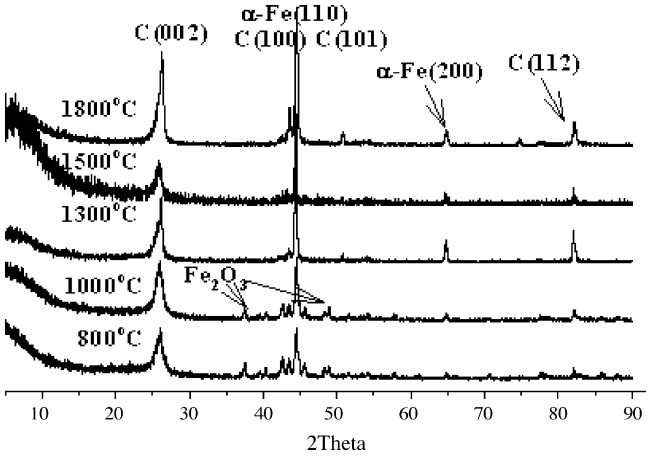

Fig. 4. WAX patterns for electrospun PVdF-based graphitic carbon nanofibers.

The crystalline structure of graphite is well characterized by Raman spectroscopy. Single hexagonal crystal graphite shows a Raman active peak at 1582 cm^{-1} (G mode) and a band around 1357 cm^{-1} can be attributed to the D mode of disorder-induced scattering, which is due to imperfection or lack of hexagonal symmetry in the carbon structure. A wide Gaussian band (M mode) is considered to represent an amorphous carbon contribution. $L_a = 4.2(I_G/I_D)$ in Raman spectra reflects the crystallite planar size of the graphite structure. Fig. 5 shows that the relative intensity (I_D/I_G) of PVdF-based GNFs rapidly decreased with increasing carbonization temperature. L_a (nm) greatly increased from 4.32 nm (800 °C) to 72.5 nm (1800 °C) with increasing carbonization temperature, as listed in Table 2. The catalytic graphitization was accelerated at >1300 °C.

Nitrogen adsorption–desorption isotherms for the GNFs were the type II showing a hysteresis loop that indicates the existence of mesopores, as shown in Fig. 6. The BET surface area and micropore volume decreased with increasing carbonization temperature as shown in Table 3. Decreases in the surface area and micropore volume are thought to be due to densification of the porous structure with increasing carbonization temperature. The GNFs showed high surface areas of 377–473 m^2/g. However, they still have low surface areas compared to typical active carbon. Table 3 also shows the surface area and micropore volume of CNFs prepared by carbonization of electrospun PVdF-based nanofibers without IAA. The latter had a very high surface area of 1300 m^2/g and a high volume (1.767 cm^3/g) of ultramicropores. Micropores are divided into supermicropores with a size of 0.7–2 nm and ultramicropores of <0.7 nm according to IUPAC [19]. Unfortunately, it is difficult to exactly analyze the ultramicropore size distribution and volume in porous carbon from nitrogen adsorption–desorption isotherm measurements compared to the diameter of hydrogen molecules. The carbonization of electrospun PVdF nanofibers is usually accompanied by the release of HF, H_2, F_2 and other gases, resulting in the formation of pores within the carbon fiber structure. In addition, micro- and mesopores are generated through the carbonization of partially dehydrofluorinated PVdF nanofibers. We assume that ultramicropores and supermicropores are generated during carbonization of the partially dehydrofluorinated PVdF nanofiber precursors. The pore structure of the GNFs became dense with increasing

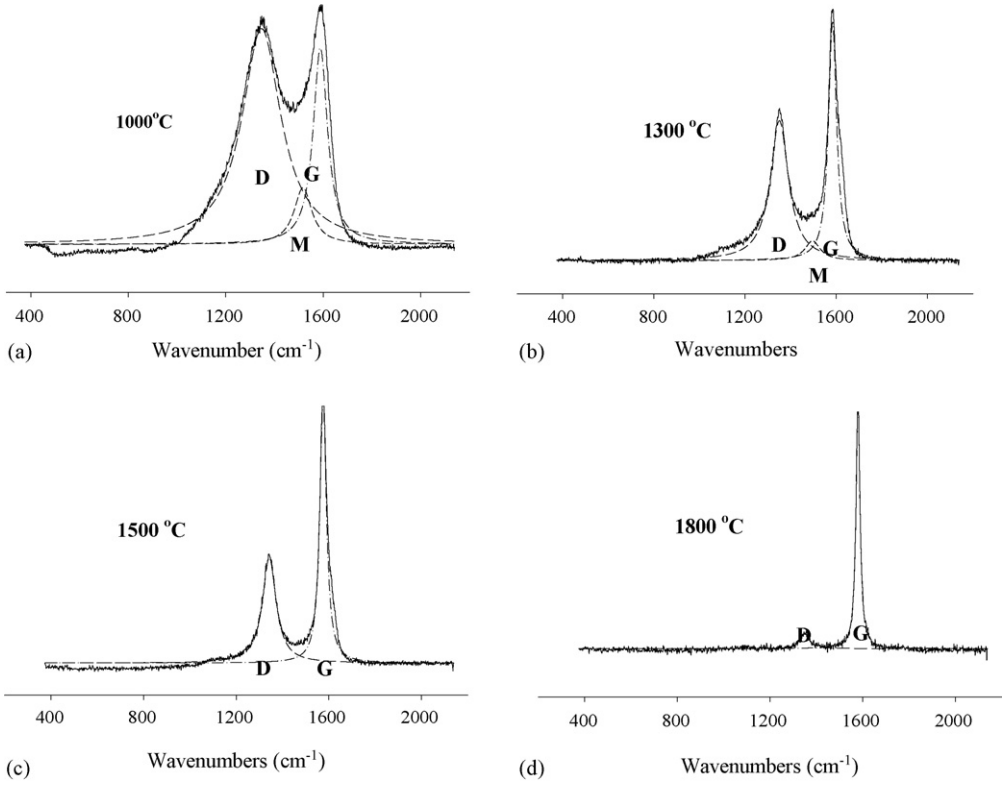

Fig. 5. Raman spectra of electrospun PVdF-based graphitic carbon nanofibers. Carbonization temperature: (a) 1000 °C; (b) 1300 °C; (c) 1500 °C; (d) 1800 °C.

Table 2
The (0 0 2) spacing values and in-plane sizes of small graphite crystals, L_a, of electrospun PVdF-based graphitic carbon nanofibers

Carbonization temperature (°C)	XRD		Raman
	2θ (°C)	$d_{0\,0\,2}$ (nm)	L_a (nm)[a]
800	26.10	0.341	4.32
1000	25.96	0.343	4.83
1300	26.12	0.341	7.50
1500	26.28	0.339	10.9
1800	26.72	0.333	72.5

[a] L_a (Raman) = 4.4 (I_G/I_D).

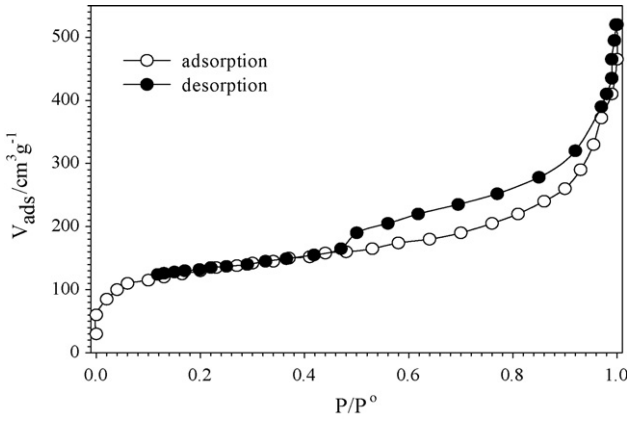

Fig. 6. Typical nitrogen adsorption–desorption isotherm for electrospun PVdF-based graphitic carbon nanofibers (carbonization temperature 1500 °C).

carbonization temperature. Therefore, an increase in carbonization temperature might lead to an increase in ultramicropore volume instead of a loss of large pores.

Fig. 7 shows hydrogen storage results for the PVdF-based GNFs under several hydrogen pressures at room temperature. The hydrogen storage capacity was measured after 2 h under a specific hydrogen pressure. The hydrogen adsorption of the GNFs increased with increase of carbonization temperature while specific surface area and micropore volume (<1 nm) were decreased. In the case of the CNF carbonized at 1800 °C it showed hydrogen storage capacity of 0.39 wt.% even though it had the highest surface area of 1300 m^2/g and highest

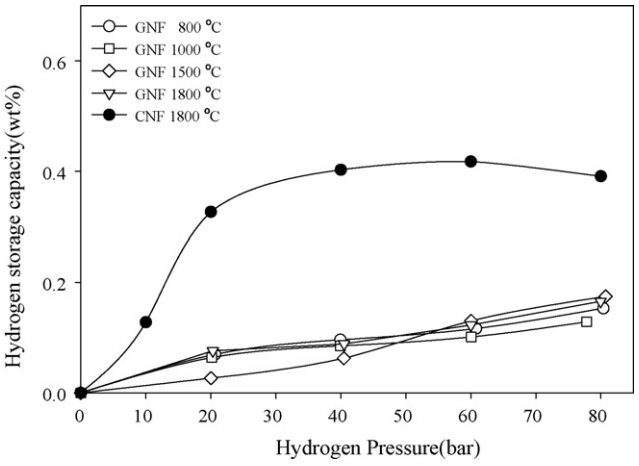

Fig. 7. Hydrogen storage capacity of electrospun PVdF-based graphitic carbon nanofibers.

ultramicropore volume of 1.767 cm^3/g. This capacity is similar to the activated carbon fibers showing 0.35–0.41 wt.% of hydrogen storage capacity [6]. The hydrogen storage capacity of the GNFs and CNFs did not show correlation with surface area or micro- and mesopore volume, as shown in Table 3. The quantity of adsorbed hydrogen on nanostructured graphitic carbon as well active carbon materials at 77 K is proportional to the specific surface area of carbon materials [8]. However, because at ambient temperature the thermal mortion of hydrogen molecules overcome van der Waals-type weak physisorption of molecular hydrogen, their hydrogen storage capacities were very low. So the hydrogen adsorption on the GNFs and CNF samples may be influenced by pore structure as well as specific surface area. Therefore, we think that micro- and mesopores that are calculated using the nitrogen gas adsorption–desorption isotherms are not the effective pore for hydrogen storage. The effective pore for hydrogen storage may require a pore size not exceeding 1 nm when considered with when compared to the diameter of hydrogen molecule (0.4059 nm). It is assumed that these micropores are different from the micropores calculated using nitrogen adsorption–desorption isotherms. Thus, hydrogen adsorption by the PVdF-based GNFs and CNFs may be due to the presence of ultramicropores rather than micro- and mesopores, even though they have very low surface areas compared to

Table 3
Specific surface areas and pore analysis for electrospun PVdF-based graphitic carbon nanofibers (GNFs)

Carbonization temperature (°C)	Total pore volume (cm^3/g)	Specific surface area (m^2/g)	Pore size distribution (cm^3/g)			
			<1 nm[a]	1–2 nm[a]	2–4 nm[b]	4–10 nm[b]
GNF						
800	0.74	473	0.162	0.042	0.132	0.294
1000	0.91	445	0.158	0.040	0.133	0.315
1500	1.01	431	0.143	0.048	0.132	0.186
1800	2.02	377	0.115	0.044	0.125	0.180
CNF						
1800	0.63	1300	1.767[c]	–	–	–

[a] Determined by applying the Horvath Kawazoe pore sizes for microporous samples.
[b] Determined by applying the B.J.H. pore sizes for mesoporous samples.
[c] Ultramicropores of below 0.8 nm.

commercially available active carbons and active carbon fibers. In the case of the GNF at 1800 °C, the reduced hydrogen storage capacity is thought to be due to the disappearance of the pore structure, including ultramicropores, at higher carbonization temperatures.

4. Conclusions

GNFs were prepared by catalytic graphitization during carbonization of electrospun PVdF-based nanofibers without further activation. The catalytic graphitization was intensively accelerated at carbonization temperatures of >1300 °C. The resulting GNFs showed a well-ordered graphite structure with $d_{0\,0\,2} < 0.34$ nm, indicating a turbostratic carbon structure.

Nitrogen adsorption–desorption isotherms of the GNFs showed type II curve in addition to a hysteresis loop that indicates the existence of mesopores. The specific surface area (377–473 m^2/g) and micropore volume decreased with increasing carbonization temperature due to densification of the porous structure.

The hydrogen storage capacity of the GNFs did not show correlation with surface area or micro- and mesopore volume calculated from the nitrogen adsorption–desorption isotherms. So the hydrogen adsorption on the GNFs and CNF samples may be influenced by pore structure as well as specific surface area. We think that micro- and mesopores that are calculated using the nitrogen gas adsorption–desorption isotherms are not the effective pore for hydrogen storage. The potential fields from opposite walls overlap so that the attractive force acting on hydrogen molecules is greater than that on an open flat surface. The effective pore for hydrogen storage may require a pore size not exceeding 1 nm when considered with when compared to the diameter of hydrogen molecule (0.4059 nm). Thus, hydrogen adsorption by the PVdF-based GNFs and CNFs may be due to the presence of ultramicropores rather than micro- and mesopores, even though they have very low surface areas compared to commercially available active carbons and active carbon fibers.

Acknowledgement

The Hydrogen Energy R&D Center in the Republic of Korea financially supported this work.

References

[1] A.C. Dillon, K.M. Jones, T.A. Bekke-Dahl, H. Kiang, D.S. Bethune, M.J. Heben, Nature 386 (1997) 377.
[2] H. Zhu, A. Cao, X. Li, C. Xu, Z. Mao, D. Ruan, J. Liang, D. Wu, Appl. Surf. Sci. 178 (2001) 50.
[3] Y. Ye, C.C. Ahn, C. Witham, B. Fultz, J. Liu, A.G. Rinzler, D. Colbert, K.A. Smith, R.E. Smalley, Appl. Phys. Lett. 74 (1999) 2307.
[4] M.G. Nijkamp, J.E.M.J. Raaymakers, A.J. van Dillen, K.P. de Jong, Appl. Phys. A 72 (2001) 619.
[5] R. Chahine, T.K. Bose, Int. J. Hydrogen Energy 19 (1994) 161.
[6] K. Kajiura, S. Tsutsui, K. Kadona, M. Ata, Appl. Phys. Lett. 82 (2003) 1105.
[7] M.G. Nijkamp, J.E.M.J. Raaymakers, A.J. Van Dillen, K.P. De Jong, Appl. Phys. A 72 (2001) 619.
[8] L. Schlapbach, A. Zuttel, Nature 414 (2001) 353.
[9] J. Yamashita, M. Shioya, T. Kikutani, T. Hashimoto, Carbon 39 (2001) 207.
[10] P.W. Gibson, H. Schreuder-Gibson, D. Rivin, Colloids Surf. A 469 (1999) 187.
[11] Y. Kaburagi, Y. Hishiyama, H. Oka, M. Inagaki, Carbon 39 (2001) 593.
[12] H. Konno, K. Shiba, Y. Kaburagi, Y. Hishiyama, M. Inagaki, Carbon 39 (2001) 1731.
[13] G.S. Chung, S.M. Jo, B.C. Kim, J. Appl. Polym. Sci. 97 (2005) 165.
[14] S.H. Park, S.M. Jo, D.Y. Kim, W.S. Lee, B.C. Kim, Synth. Met. 150 (2005) 265.
[15] D.K. Kim, S.H. Park, B.D. Chin, S.M. Jo, D.Y. Kim, B.C. Kim, Macromol. Res. 13 (6) (2005) 521.
[16] H.J. Chung, S.M. Jo, D.Y. Kim, B.D. Chin, D.W. Lee, Trans. Korean Hydrogen New Energy Soc. 16 (4) (2005) 334.
[17] A. Goto, M. Kyotani, K. Tsugawa, G. Piao, K. Akagi, Y. Koga, Carbon 41 (2003) 131.
[18] Y. Hishiyama, K. Igarashi, I. Kaneko, T. Fujii, T. Kaneda, T. Koidezawa, Y. Shimazawa, A. Yoshida, Carbon 35 (1997) 657.
[19] M. Inagaki, New Carbons: Control of Structure and Functions, Elsevier Science Ltd., 2000,, p. 82.